IEEE Photonics Journal
An IEEE Photonics Society Publication

Open Access

Si-Ge-Silica Monolithic Integration Platform and Its Application to a 22-Gb/s × 16-ch WDM Receiver

Volume 5, Number 4, August 2013

Tatsurou Hiraki
Hidetaka Nishi
Tai Tsuchizawa
Rai Kou
Hiroshi Fukuda
Kotaro Takeda
Yasuhiko Ishikawa
Kazumi Wada
Koji Yamada

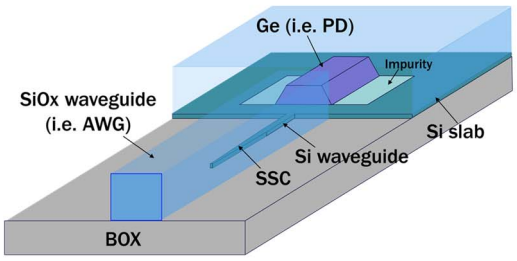

Si-Ge-silica monolithic integration platform

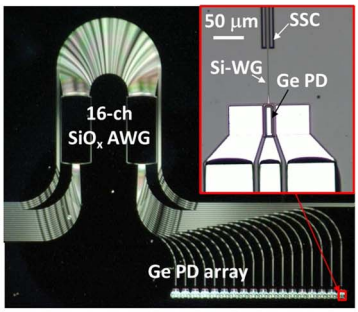

22-Gb/s x 16-ch WDM receiver

DOI: 10.1109/JPHOT.2013.2269676
1943-0655/$31.00 ©2013 IEEE

IEEE photonics SOCIETY

IEEE

Si-Ge-Silica Monolithic Integration Platform and Its Application to a 22-Gb/s × 16-ch WDM Receiver

Tatsurou Hiraki,[1,2] Hidetaka Nishi,[1,2] Tai Tsuchizawa,[1,2] Rai Kou,[1,2] Hiroshi Fukuda,[1] Kotaro Takeda,[1,2] Yasuhiko Ishikawa,[3] Kazumi Wada,[3] and Koji Yamada[1,2]

[1]NTT Microsystem Integration Laboratories, NTT Corporation, Atsugi 243-0198, Japan
[2]Nanophotonics Center, NTT Corporation, Atsugi 243-0198, Japan
[3]Department of Materials Engineering, University of Tokyo, Tokyo 113-8656, Japan

DOI: 10.1109/JPHOT.2013.2269676

Manuscript received April 11, 2013; revised May 31, 2013; accepted June 5, 2013. Date of current version July 2, 2013. Corresponding author: T. Hiraki (e-mail: hiraki.tatsurou@lab.ntt.co.jp).

Abstract: We describe a Si–Ge–silica monolithic integration platform for telecommunications applications. The monolithic integration process features low-temperature silica film deposition by electron-cyclotron-resonance chemical vapor deposition to prevent thermal damage to Si/Ge active devices. The monolithically integrated Si and SiOx waveguides show propagation losses of 2.8 and 0.9 dB/cm, and the inverse-tapered spot-size converters show a coupling loss of 0.35 dB. We applied the platform to a 22-Gb/s × 16-ch wavelength-division multiplexing receiver, in which a 16-ch SiOx arrayed waveguide grating (AWG) with 1.6-nm channel separation and Ge photodiodes (PDs) are monolithically integrated. The AWG-PD device exhibits fiber-to-PD responsivity of 0.29 A/W and interchannel crosstalk of less than −22 dB and successfully receives 22-Gb/s signal for all 16 channels. In addition, we demonstrate 40-km transmission of 12.5-Gb/s signal and obtain sensitivity of −6.8 dBm at a bit error rate of 10^{-9} without transimpedance amplifiers.

Index Terms: Silicon nanophotonics, waveguide devices.

1. Introduction

Towards the next generation of broad-band optical networks, often referred to as NG-PON2, revolutionary network technology is under discussion, and innovative cost-effective long-term solutions are required [1]–[3]. Among the many proposed systems, those based on wavelength-division multiplexing (WDM) are expected to offer flexible bandwidth allocation, which contributes to energy-efficient network operation [4]. A wavelength selectable receiver is a key component of such WDM-based systems. Recently, several WDM receivers with high capacity of up to several hundred gigabits per second have been developed by using a silicon (Si) photonics platform. The Si photonics platform is widely expected to provide small, cost-effective photonic-electronic integrated circuits with high-functionality. On the platform, wavelength filters must meet several severe requirements, including low insertion loss, low crosstalk, and insensitivities to polarization and temperature. Although several wavelength filters based on Si waveguides are reported [5], [6], they could not meet such requirements due to polarization and temperature sensitivities. We must carefully select waveguide materials. For example, silicon nitride (SiN) waveguides fabricated on the Si platform was reported [7], [8] for the high performance wavelength filter. The monolithically integrated SiN arrayed-waveguide-grating (AWG) with germanium (Ge) photodiodes (PDs) showed

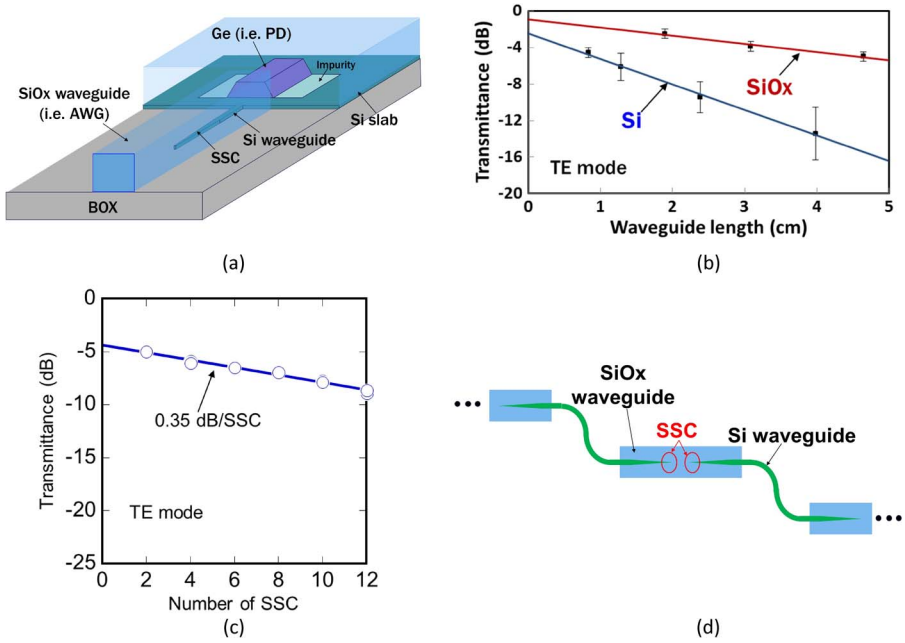

Fig. 1. (a) Schematic of Si-Ge-silica monolithic integration platform for Ge PD. (b) Transmission characteristics of Si and SiOx waveguides. (c) Relationship between transmittance and the number of SSCs. (d) Schematic of sample for SSC-loss measurement.

the low loss and the high responsivity, but the large crosstalk, polarization sensitivity, and some thermo-optic effect still remained [8]. The most promising solution is to use silica waveguides, which have low loss, low polarization dependence, and a low thermo-optic coefficient. Planar lightwave circuits (PLCs) based on silica AWGs meet telecom requirements and have been used in existing optical telecommunications networks [9], [10]. However, the high-temperature fabrication processes for the commercial silica PLC could not be used for the Si photonic platform because of thermal damages to Si/Ge active devices. To integrate the silica wavelength-filter with Si/Ge active devices, in previous work, we have developed a Si-Ge-silica monolithic photonic integration platform [11], [12]. On the platform, low-loss and low-temperature-dependent silica passive devices and compact high-speed Si/Ge active devices are monolithically integrated with low-loss inverse-tapered spot-size converters (SSCs). The platform is suitable for the next generation of wavelength-selectable receivers. In this paper, we report the details of the Si-Ge-silica monolithic integration platform and its application to a broadband WDM receiver, which comprises a 16-ch silica-based AWG and 22-Gb/s Ge-PD arrays.

2. Si-Ge-Silica Monolithic Photonic Integration Platform

Fig. 1(a) shows a schematic image of the Si-Ge-silica monolithic integration platform. Si waveguides, SSCs [13], Ge active devices (i.e., PDs), and silica waveguides (i.e., AWG) are monolithically fabricated on a silicon-on-insulator (SOI) wafer. The monolithic integration process features a low-temperature formation of silica waveguides using the electron-cyclotron-resonance (ECR) chemical vapor deposition (CVD), which prevents thermal damage to Si/Ge active devices. The ECR CVD enables us to control refractive indexes of Si-rich silica-based films (SiOx films) and silicon-oxynitride films (SiOxNy films) at 150 degrees Celsius [12], because ECR plasma easily dissociates gas molecules. Table 1 shows the atomic percentages of the core- and clad-films of the SiOx- and SiOxNy-waveguides with refractive-index differences (deltas) of $\sim$2.9%. The atomic percentages were measured by Rutherford backscattering spectrometry (RBS), and we confirmed that the composition of the thermal-oxide film (reference) was precisely measured to be $SiO_{2.0}$ by the technique. The compositions of the SiOx core, the SiOxNy core, and the clad films were $SiO_{1.7}$,

TABLE 1

Atomic percentages of core and clad films

Sample name	Refractive index	Si (%)	O (%)	N (%)	Others (%)
SiOx core	1.52	34.1	57.6	-	8.3
SiOxNy core	1.51	32.0	59.0	4.9	4.1
Clad	1.47	30.7	62.6	-	6.7
Thermal oxide	1.46	33.8	66.2	-	-

$SiO_{1.8}N_{0.2}$, and $SiO_{2.0}$, respectively. These results show that the refractive indexes of the silica-based films were successfully controlled by the atomic ratio of Si/O (N). Here, for the WDM devices, the SiOx core was used for most of the passive devices because it has lower optical absorption in the C-band than the SiOxNy core. In addition to the ECR-CVD, the monolithic integration process has the following features with respect to the formation of low-loss waveguides. First, Si cores and Si tapers in SSCs are fabricated using electron beam lithography and ECR plasma etching [11]. These processes provide low side-edge-roughness and small process damage to Si. Second, the Ge film is formed by selective growth on Si using ultrahigh-vacuum (UHV) CVD and post growth annealing [14]. This technique forms low-dislocation-density Ge-films without contamination to the waveguides.

Fig. 1(b) shows transmission characteristics of monolithically integrated Si and SiOx waveguides with a delta of 2.9%. The core size of the Si and the SiOx waveguides are 200-nm $\times$ 400-nm and 3 μm $\times$ 3 μm, respectively. The input light source was amplified spontaneous emission (ASE) light with the transverse electric (TE) mode. From a linear fitting of the averaged transmittance, the propagation losses of the Si and SiOx waveguides were estimated to be 2.8 and 0.9 dB/cm, respectively. The polarization depended propagation loss of the SiOx waveguides is typically less than 0.1 dB/cm [15]. Fig. 1(c) shows relationships between transmittance and the number of SSCs between Si and SiOx waveguides. In the measurement sample, several numbers of SSCs are connected between Si and SiOx waveguides, as shown in Fig. 1(d). The size of the taper tip of the SSCs is 200-nm $\times$ 80-nm, which shows a reflection ratio at the taper region of less than -40 dB [12]. The measurement results show that the coupling loss per SSC is 0.35 dB with TE mode light, which is low enough to meet severe telecommunications-grade requirements on the platform. We also measured a coupling loss with TM mode light. The TM-mode coupling loss per SSC is 0.31 dB. The inversed taper SSCs show the polarization insensitivities.

3. Application to Broadband WDM Receiver

In this work, we applied the platform to a broadband WDM receiver, which comprised 16-ch SiOx-AWG and 22-Gb/s Ge-PD arrays (22-Gb/s $\times$ 16-ch). Fig. 2(a) shows a top view image of the AWG-PD device. The channel spacing of the AWG is 200 GHz (wavelength of $\sim$1.6 nm). The polarization-depended wavelength shift $(\mathrm{PD}\lambda)$ of the SiOx AWG due to a film stress could be compensated by a multi-layer core [15]. However, in this work, we used a single-layer SiOx core for a feasibility check of the integration process, so the AWG has a PDλ of $\sim$2.0 nm. The SiOx AWG is connected to Ge PDs through SSCs and Si waveguides, as shown in inset of Fig. 2(a). The length of the Si waveguides was 100 μm; therefore, their insertion loss was only about 0.28 dB, which was negligible in terms of the total loss of the AWG-PD chip. The cross-sectional view of the Ge PD on the Si waveguide is shown in Fig. 2(b). We designed to reduce parasitic resistance at the n-Ge/electrode interface because, in our previous work, the high n-Ge-contact resistance limited the operation speed to 1.25 Gb/s [11]. In this work, we used a Ti/n-Si contact film to prevent Fermi-level pinning and form an ohmic contact [16]. Here, the thickness of the Ge film was 1 μm, and the Ge area was 10 μm $\times$ 50 μm.

For the monolithic integration of Ge active devices with the Si and SiOx waveguides, we developed the following fabrication process for the AWG-PD chip: First, Si cores and Si tapers in

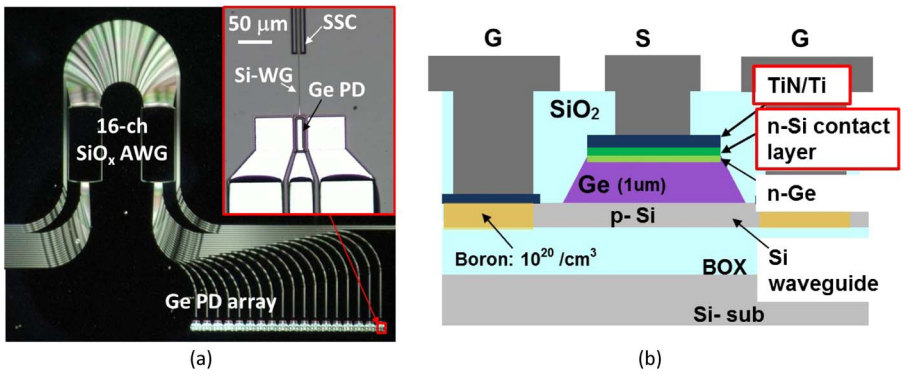

Fig. 2. (a) Top view of the AWG-PD device; (b) cross section of Ge PD.

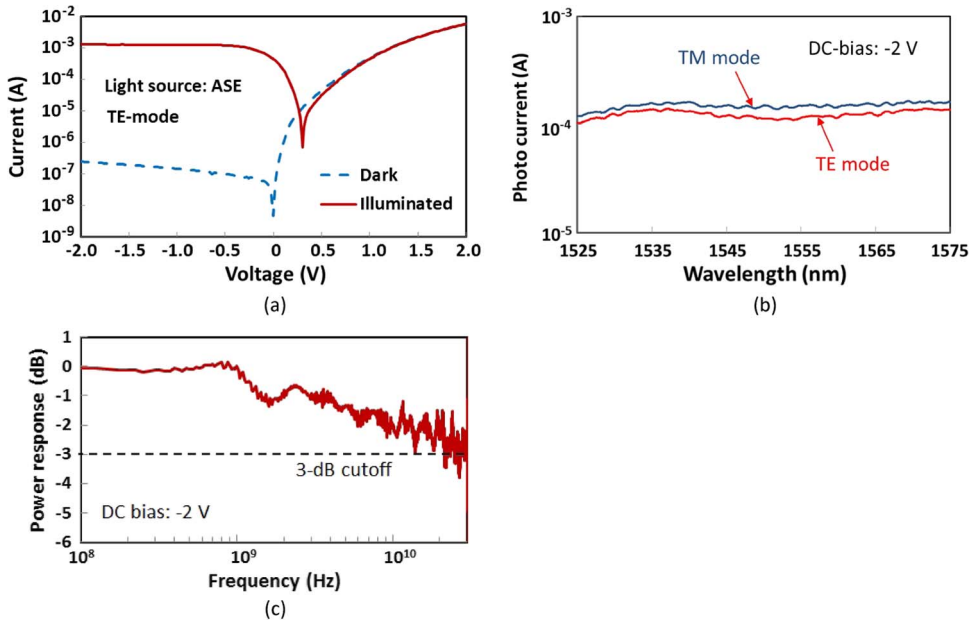

Fig. 3. (a) Current-voltage curves of the Ge PD. (b) Wavelength dependence of the photocurrent of Ge PD with TE and TM mode input. (c) Frequency response of the Ge PD.

SSCs were fabricated on the SOI wafer with a 3-μm-thick buried-oxide and 200-nm-thick Si layer. Next, boron implantation and Ge selective growth for Ge PDs were performed. After the Ge growth, a thin Si film was deposited on the Ge surface to prevent the Ge film from being damaged during the CMOS process. After that, a SiOx film was formed by using ECR CVD for the SiOx AWG. The SiOx film was then etched to form cores for the AWG and SSCs, and phosphine was implanted into the Si/Ge layer on top of the Ge PD. After that, an over-cladding SiO_2 film was deposited and contact-holes were formed. Finally, Ti/TiN/Al electrodes were formed.

First, the performance of a stand-alone Ge PD with Si/SiOx waveguides was evaluated. Fig. 3(a) shows current-voltage curves of the Ge PD in the dark and the illuminated state. Input light power was 1.26 mW at the SSC before the Ge PD. Dark current and photocurrent were 245 nA and 1.27 mA at a DC bias of -2 V. The responsivity of the stand-alone PD is estimated to be about 1.0 A/W at the entrance of the SSC. Although the responsivity includes the losses of the SSC and the 100-μm-length Si waveguide, it is high enough for the WDM receiver. The relationship between photocurrent and wavelength is shown in Fig. 3(b). Ge PDs show flat wavelength dependence in the C-band, and the

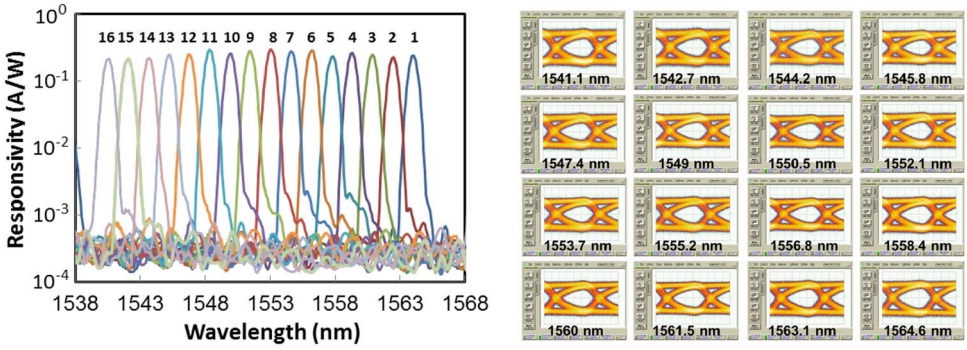

Fig. 4. (a) DEMUX spectra of the AWG-PD chip; (b) eye diagrams of DEMUX photocurrent with 22-Gb/s signal for all channels.

polarization dependence of the power amplitude is less than 1.0 dB. The small wavelength and polarization dependence is suitable to the WDM receiver. The series resistance of the PD is estimated to be $\sim 140\ \Omega$ by a linear fitting. This value is about ten times lower than that in the previous work [11]. The low parasitic resistance provides to reduce RC delay and improves the operation speed of the PD. The frequency response of the Ge PD is shown in Fig. 3(c). The 3-dB cutoff frequency of the Ge PD at DC bias of -2 V was estimated to be about 20 GHz.

We evaluated performance of the monolithically integrated AWG-PD device. We input TE-mode light from tunable laser diodes (TLDs) into the silica AWG and obtained demultiplexing (DEMUX) spectra from all 16 channels of Ge PDs at DC bias of -2 V while sweeping the TLD wavelength. DEMUX spectra are shown in Fig. 4(a). The spectra show a channel spacing of $\sim$1.6 nm as designed, and interchannel crosstalk is less than -22 dB. The insertion loss of the AWG at the central wavelength is about 5.1 dB, which includes waveguide propagation loss of $\sim$1.8 dB and diffraction loss of $\sim$3.3 dB. The fiber-to-waveguide coupling loss is 0.48 dB/facet. The fiber-to-PD responsivity, which is normalized at the input power before the AWG, is 0.29 A/W at the central wavelength. The monolithic integration of the high-performance SiOx AWG with Ge PDs contributes a lower crosstalk and higher responsivity than those in other reports, which are the Si AWG with Ge PDs [6] and the SiN AWG with Ge PDs [8]. Next, we input non-return to zero (NRZ) pseudo-random bit sequence (PRBS) data with pattern length of $2^{31} - 1$ into the AWG and measured eye diagrams of 16-ch Ge PDs at DC bias of -2 V. We input TE mode light with a sufficiently large power, which was over $\sim$0 dBm at the Ge PDs. The eye diagrams of DEMUX photocurrent with 22-Gb/s signal inputs for all channels are shown in Fig. 4(b). We confirmed that all 16 channels showed clear opening eyes. The AWG-PD chip achieves total system bandwidth of 352 Gb/s. Here, the bit rate was limited to 22 Gb/s by the measurement equipment. Because the bandwidth could be smaller than the bit rate, the Ge PDs whose bandwidth are 20 GHz operate fast enough for 25 Gb/s [17]; therefore, the total system bandwidth could potentially reach 400 Gb/s.

To confirm the feasibility of the AWG-PD device for practical network applications, we examined long-distance transmission. Fig. 5(a) shows the experimental setup. Continuous-wave infrared light from TLDs was modulated by a lithium-niobate Mach-Zehnder modulator (MZM). The modulation format is simple intensity modulation with 12.5-Gb/s NRZ PRBS data. The word length was $2^{31} - 1$. The signal bandwidth was restricted to 12.5 Gb/s by our experimental equipment. The modulated optical signal was transmitted through standard single-mode fibers (SSMFs) with dispersion of 17 ps/km/nm at distances of 20, 40, and 60 km. Then, to emulate a real receiver, we introduced a commercial clock-data recovery (CDR) module. The input signal was tapped by a 10-dB coupler and guided into the CDR module. After polarization preparation, the signal was input into the AWG-PD device by butt coupling of a high-NA fiber. The experiment was performed at room temperature without temperature control. The electrical signals from Ge PDs were detected by an oscilloscope (OSC). The signal was also put into an error detector (ED) for bit-error rate (BER) measurement

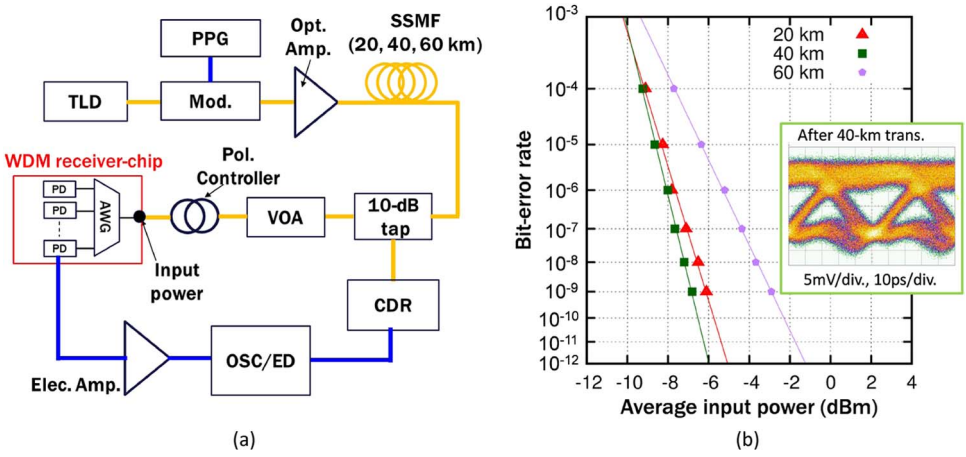

Fig. 5. (a) Experimental setup; (b) BER curves of channel 12 for various transmission distances and eye diagram after 40-km transmission (inset).

without transimpedance amplifiers (TIAs). The recovered clock was distributed from the CDR module to the OSC and ED.

Fig. 5(b) shows measured BER curves obtained from channel 12 for various transmission distances and a received eye diagram after 40-km transmission (inset). The channel numbers are shown in Fig. 4(a). We confirmed error-free signal transmission up to 40 km. The receiver sensitivity measured at the AWG input was -6.8 dBm for the BER of 10^{-9} after 40-km transmission. After 60-km transmission, the BER was increased considerably by waveform distortion due to the dispersion and nonlinearity of the fiber. Taking into account the transmission loss of the AWG, we estimated the sensitivity of the Ge PD on channel 12 to be -13.6 dBm for the 40-km transmission. Although the theoretical sensitivity of the AWG-PD device is -32 dBm, estimated from a shot- and Johnson-noise [17], the measured sensitivity was restricted by the measurement system, in that there were no TIAs in this chip. We believe the sensitivity will be improved by on-chip integration of TIAs, which, as we reported previously, has been already carried out [11]. Finally, one should note that temperature insensitivity of the silica AWG benefits us and the wavelength channels were stable enough even though these experiments were performed without thermal control.

4. Conclusion

We reported a Si-Ge-silica monolithic integration platform for telecommunications applications. The monolithic integration process features the low-temperature silica film deposition by ECR CVD to prevent thermal damage to Si/Ge active devices. The monolithically integrated Si and SiOx waveguides showed propagation losses of 2.8 and 0.9 dB/cm, and the inverse-tapered SSCs showed coupling losses of 0.35 dB with TE-mode light. The PDLs of the SiOx waveguide and SSCs are $\sim$0.1 dB/cm and $\sim$0.04 dB, respectively. We applied the platform to a 22-Gbit/s $\times$ 16-ch AWG-PD device. The Ge PD is designed with the n-Si contact layer at the n-Ge/meal interface for a small RC delay. The stand-alone Ge PD with the Si/SiOx waveguides and the SSC showed a bandwidth of $\sim$20 GHz and a responsivity of 1.0 A/W. The polarization dependence of the photocurrent-power amplitude is less than 1.0 dB, which is contributed by the low polarization sensitivities of the SiOx waveguide and the SSC. The integrated AWG-PD device exhibited fiber-to-PD responsivity of 0.29 A/W and inter-channel crosstalk of less than -22 dB and successfully received 22-Gbit/s signal for all 16 channels. In addition, we demonstrated 40-km transmission of 12.5-Gbit/s signal using a fabricated receiver chip, and sensitivity of -6.8 dBm at BER of 10^{-9} was obtained. TIA integration on the photonic chip enables us to improve this sensitivity further, and this Si-Ge-silica integration platform provides a dense integrated WDM receiver for future telecommunications applications.

Acknowledgment

We thank T. Watanabe, Y. Muramoto, H. Tanobe, K. Hasebe, M. Nogawa, Y. Doi, M. Takahashi, and S. Itabashi for their technical support and valuable discussions.

References

[1] J. Kani, "Power saving techniques for optical access," presented at the Proc. OFC/NFOEC, Los Angeles, CA, USA, 2012, Paper NM2K.1.
[2] R. Murano and M. J. Cahill, "Low cost tunable receivers for wavelength agile PONs," presented at the Proc. ECOC, Amsterdam, The Netherlands, 2012, Paper We.2.B.3.
[3] F. Bourgart, "NGPON2—Where are the standards going?" in *Proc. OFC/NFOEC*, Los Angeles, CA, USA, 2012, Paper NTu2F.3.
[4] K. Hara, H. Nakamura, S. Kimura, M. Yoshino, S. Nishihara, S. Tamaki, J. Kani, N. Yoshimoto, and H. Hadama, "Flexible load balancing technique using dynamic wavelength bandwidth allocation (DWBA) toward 100 Gbit/s-class-WDM/TDM-PON," in *Proc. ECOC*, Torino, Italy, 2009, Paper Tu.3.B.2.
[5] D. Feng, W. Qian, H. Liang, N. Feng, S. Liao, C. Kung, J. Fong, Y. Liu, R. Shafiiha, D. C. Lee, B. J. Luff, and M. Asghari, "Terabit/s single chip WDM receiver on the SOI platform," in *Proc. IEEE Int. Conf. Group IV Photon.*, 2011, pp. 320–322.
[6] J. M. Fedeli, L. Virot, J. M. Hartmann, P. Grosse, W. Bogaerts, and L. Vivien, "16 channel receiver with 20 GHz Ge photodiodes," in *Proc. IEEE Int. Conf. Group IV Photon.*, 2012, pp. 156–158.
[7] C. R. Doerr, L. Chen, L. L. Buhl, and Y. K. Chen, "Eight-channel $SiO_2/Si_3N_4/Si$/Ge CWDM receiver," *IEEE Photon. Technol. Lett.*, vol. 23, no. 17, pp. 1201–1203, Sep. 2011.
[8] L. Chen, C. R. Doerr, L. Buhl, Y. Baeyens, and R. A. Aroca, "Monolithically integrated 40-wavelength demultiplexer and photodetector array on silicon," *IEEE Photon. Technol. Lett.*, vol. 23, no. 13, pp. 869–871, Jul. 2011.
[9] T. Miya, "Silica-based planar lightwave circuits: Passive and thermally active devices," *IEEE Sel. Topics Quantum Electron.*, vol. 6, no. 1, pp. 38–45, Jan./Feb. 2000.
[10] C. Doerr and K. Okamoto, "Advances in silica planar lightwave circuits," *J. Lightw. Technol.*, vol. 24, no. 12, pp. 4763–4789, Dec. 2006.
[11] H. Nishi, T. Tsuchizawa, R. Kou, H. Shinojima, T. Yamada, H. Kimura, Y. Ishikawa, K. Wada, and K. Yamada, "Monolithic integration of a silica AWG and Ge photodiodes on Si photonic platform for one-chip WDM receiver," *Opt. Exp.*, vol. 20, no. 8, pp. 9312–9321, Apr 2012.
[12] T. Tsuchizawa, K. Yamada, T. Watanabe, S. Park, H. Nishi, R. Kou, H. Shinojima, and S. Itabashi, "Monolithic integration of silicon-, germanium-, and silica-based optical devices for telecommunications applications," *IEEE J. Sel. Topics Quantum Electron.*, vol. 17, no. 3, pp. 516–525, May/Jun. 2011.
[13] T. Shoji, T. Tsuchizawa, T. Watanabe, K. Yamada, and H. Morita, "Spot-size converter for low-loss coupling between 0.3-mm-square Si wire waveguides and single-mode fibers," in *Proc. LEOS*, 2002, vol. 1, pp. 280–290.
[14] S. Park, Y. Ishikawa, T. Tsuchizawa, T. Watanabe, K. Yamada, S. Itabashi, and K. Wada, "Effect of post-growth annealing on morphology of Ge mesa selectively grown on Si," *IEICE Trans. Electron.*, vol. E91-C, no. 2, pp. 181–186, Jan. 2008.
[15] H. Nishi, T. Tsuchizawa, H. Shinojima, T. Watanabe, S. Itabashi, R. Kou, H. Fukuda, and K. Yamada, "Low-polarization-dependent silica waveguide monolithically integrated on SOI photonic platform," *J. Lightw. Technol.*, vol. 31, pp. 1821–1827, 2013.
[16] T. Nishimura, K. Kita, and A. Toriumi, "Evidence for strong Fermi-level pinning due to metal-induced gap states at metal/germanium interface," *Appl. Phys. Lett.*, vol. 91, no. 12, p. 123 123, Sep. 2007.
[17] G. Agrawal, *Fiber-Optic Communication Sytems,* 2nd ed. New York, NY, USA: Wiley, 1997.